Optics and Laser Technology 121 (2020) 105826

Contents lists available at ScienceDirect

Optics and Laser Technology

journal homepage: www.elsevier.com/locate/optlastec

Research Note

Polarization-sensitive terahertz resonator using asymmetrical F-shaped metamaterial

Zhicheng Lin, Zefeng Xu, Pengyu Liu, Zihao Liang, Yu-Sheng Lin*

State Key Laboratory of Optoelectronic Materials and Technologies, School of Electronics and Information Technology, Sun Yat-Sen University, Guangzhou 510275, China

HIGHLIGHTS

- Tunable THz resonator using asymmetrical F-shape metamaterial (AFSM) is presented.
- AFSM exhibits switching function for single-band and dual-band resonances.
- AFSM can be modulated as single-resonance or dual-resonance at different polarization mode.
- AFSM exhibits ultra-narrow bandwidth with highest Q-factor of 40.
- AFSM can be used as high-efficiency environmental sensor.

ARTICLE INFO

Keywords:
Metamaterial
THz modulator
THz resonator

ABSTRACT

A design of tunable terahertz (THz) resonator by using asymmetrical F-shaped metamaterial (AFSM) is presented, which is composed of Au layer fabricated on silicon-on-insulator (SOI) substrate. There are three designs of AFSM with different length of F-shaped microstructure, which are 60 μm, 65 μm, and 70 μm kept other parameters as constant. The electromagnetic response of tunable THz resonator exhibits the switch function for single-band resonance at transverse magnetic (TM) mode and dual-band resonance at transverse electric (TE) mode by changing the gap between AFSM microstructures. These characterizations of device can be used for a THz filter at TM mode and a THz switch at TE mode. To compare the proposed AFSM device with and without a gap, that can be switched in the range of 0.20–0.40 THz for single-band switching resonance at TM mode and dual-band switching resonance at TE mode, respectively. These resonances are ultra-narrow bandwidths with a highest Q-factor of 40 at TE mode and kept as stable at 20 at TM mode. Such results are very suitable to be used for an environmental sensor. To further enhance the flexibility of AFSM device, it is exposed on ambient environment with different refraction index for high-efficiency environmental sensor with a correlation coefficient of 0.9999. This study paves a way to the possibility of high-sensitivity of tunable THz metamaterial in filter, switch, polarizer, and other applications.

1. Introduction

Terahertz (THz) optics in spectroscopy and imaging systems are essential to THz wave applications in physics study, quality control, security check, molecule identification, and so on [1–3]. However, THz optics in-between the light source and photodetector becomes a bottleneck owing to many dielectrics and semiconductors are penetrable by THz wave. By contrast, the integration of THz optics constituted by miniaturized optical components are expected to express higher signal transmission or reflection [4,5]. It allows more compact systems and enables the integration with other systems for increasing flexibility and applicability. For example, THz device can be compacted into semiconductor integrated circuits and integrated photonic circuits [6,7]. Such miniaturized THz devices are required alternative approaches and techniques to possess actively THz-wave manipulation and multi-functionalities.

Transformation optics is one of the key theories to describe the propagation path of electromagnetic wave [8]. Recently, metamaterials have attracted extensive research interest due to their unique optical properties that cannot be found in natural materials. In view of that, THz metamaterial becomes a feasible material for electro-optics applications. Owing to the unusual properties of metamaterial, metamaterial-based devices exhibit many advantages in place of traditional optical devices, such as filter, waveguides, polarizer, resonator, and

* Corresponding author.
E-mail address: linyoush@mail.sysu.edu.cn (Y.-S. Lin).

https://doi.org/10.1016/j.optlastec.2019.105826
Received 30 April 2019; Received in revised form 4 August 2019; Accepted 6 September 2019
Available online 13 September 2019
0030-3992/

switch [9–14]. There are a lot of literatures widely reported THz metamaterials by using symmetrical or asymmetrical split-ring resonator (SRR) to perform THz filter, THz polarizer, and THz switch [12–18]. The configurations are included but not limited to electric SRR (eSRR) [19], spiral-shaped SRR [20], U-shaped SRR [21], complementary SRR (cSRR) [22], V-shaped SRR [23], flexible SRR [24], and so on. However, the corresponding resonances of these designs can be only filter or absorb certain frequency passively. To improve the flexibility of THz metamaterial, there are many literatures reported and demonstrated many tuning mechanisms, including optical [25], electrical [26], magnetic [27], thermal [28], and mechanical [29] approaches. These reported tuning mechanisms are limited to a single application caused from the symmetric or asymmetric SRR configurations. For example, the design of THz filter is improbable for the use of THz switch and polarizer. Furthermore, the quality factor (Q-factor) of reported THz devices are limited to be very low (~0.5–5) [19–31]. On account of this, the desire to achieve a multifunctional THz device with high Q-factor and active tunability has been a research topic of interest for scientists.

In this study, we propose a tunable THz resonator composed of asymmetrical F-shaped metamaterial (AFSM). This design exhibits multi-functionalities and ultrahigh Q-factor. AFSM can be not only tuned from single-band to dual-band resonance at TE mode for filter and switch, but also tuned between TE and TM modes for polarizer. To increase the flexibility of AFSM device, it is exposed on ambient environment with different refraction index for high-efficiency environmental sensor application. The relationship of resonance and refraction index is quite linear. The corresponding correlation coefficient is 0.9999. This design of tunable AFSM opens an avenue to the possibility of THz wave manipulations for the uses in filter, resonator, switch, and other THz applications [32–38].

2. Materials and methods

Fig. 1 shows the schematic drawing of proposed tunable AFSM composed of an Au layer with 300 nm in thickness on silicon-on-insulator (SOI) substrate. The corresponding geometrical denotations of unit cell are illustrated, where $P_x = 125\,\mu m$, $P_y = 60\,\mu m$, $a = 40\,\mu m$, $c = 5\,\mu m$, $d = 10\,\mu m$ are kept as constant in this study. Three designs of AFSM are $b = 60\,\mu m$, $b = 65\,\mu m$, and $b = 70\,\mu m$, respectively, while x parameter is changed from 0 μm to 40 μm. The resonant frequency of AFSM can be tuned by using MEMS-based actuation force to change x parameter, e.g. electrothermal or electrostatic force. The optical responses of AFSM are adapted using full-field electromagnetic wave simulations performed by commercial simulation software Lumerical, three-dimensional finite difference time-domain (FDTD) solutions. The background index and surrounding temperature are set as 1 and 300 K, respectively. In addition, the simulated integration time is set as 100 ps.

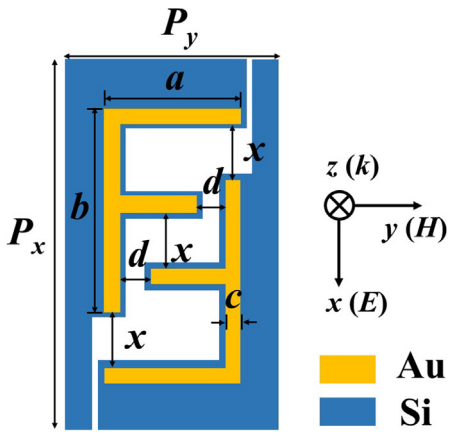

Fig. 1. Schematic drawing of THz resonator using AFSM.

According to the Drude-Lorentz model theory, the resonance of AFSM is a function of the refractive index of electromagnetic wave expressed by $n_{EM} = \sqrt{\varepsilon(\omega)\mu(\omega)}$, which can be calculated by using equation (1).

$$n_{EM} = \sqrt{\left(1 - \frac{F\cdot\omega_{pe}^2}{\omega^2 - \omega_{LCe}^2}\right)\left(1 - \frac{F\cdot\omega_{pm}^2}{\omega^2 - \omega_{LCm}^2}\right)} \quad (1)$$

where ω_{LC} is LC resonance, ω_p is dipole resonance, and F is a dimensionless quantity, while subscripts e and m refer to electric and magnetic response [39]. Periodic boundary conditions are adopted in the x and y directions and perfectly matched layer (PML) boundaries conditions are assumed in the z direction. The transmission (T) of THz waves are calculated by setting two monitors on both sides of device. AFSM with gaps, i.e. x parameters between double F-shaped microstructures can be considered as an inductive-capacitive (LC) resonator from the view of equivalent circuit [40]. The inductance and capacitance are related to the contour and gap of AFSM, respectively. The electromagnetic resonance of AFSM is a function of refraction index of THz wave, according to the quasi-static formulas for a parallel plate capacitor and a solenoid. The inductance and capacitance in the formula can be expressed as $C = \varepsilon_0\varepsilon_c ct/x$ and $L = \mu_0 b^2/t$, where ε_0 is the free space permittivity, and ε_c is the relative permittivity of the materials within gap, t is the metallic thickness. The resonant frequency can be obtained by [41]

$$f_{LC} = \frac{1}{2\pi\sqrt{LC}} = \left(\frac{1}{2\pi b\sqrt{\varepsilon_0\varepsilon_c\mu_0}}\right)\sqrt{\frac{x}{c}} \quad (2)$$

Therefore, the resonant frequency of AFSM can be actively tuned to blue-shift by increasing x value.

3. Results and discussions

Fig. 2 shows the transmission spectra of AFSM by changing x parameter from 0 μm to 40 μm at TE and TM modes as shown in Fig. 2(a) and (b), respectively. The geometrical dimensions are kept as $b = 60\,\mu m$, $a = 40\,\mu m$, $c = 5\,\mu m$, and $d = 10\,\mu m$. In the initial state, the gap between AFSM is zero, i.e. $x = 0\,\mu m$, the resonances of AFSM are 0.26 THz and 0.33 THz at TE mode and TM mode, respectively. When x value is changed from 4 μm to 40 μm, there are two resonances at TE mode. The first resonance is kept as constant as 0.21 THz and second resonance is shifted from 0.33 THz to 0.38 THz. The tuning range is 0.05 THz. It is clearly observed that AFSM exhibits a single-band and dual-band switching characteristic. At TM mode, there is one resonance shifted from 0.33 THz to 0.44 THz for x value changing from 0 μm to 40 μm. The trend of tuning resonance is nonlinear with a tuning range of 0.11THz. The transmission spectra of AFSM with b parameter of 65 μm and other parameters are kept as constant as $a = 40\,\mu m$, $c = 5\,\mu m$, and $d = 10\,\mu m$ at TE and TM modes as shown in Fig. 3(a) and (b), respectively. In the initial state, the gap between AFSM is zero, the resonances of AFSM are 0.26 THz and 0.33 THz at TE mode and TM mode, respectively. When x value is changed from 4 μm to 40 μm, the first resonance is almost kept as constant as 0.21 THz and the second resonance is shifted from 0.33 THz to 0.38 THz. The tuning range is 0.05 THz. When the x value is 0 μm, there is only one resonance at 0.26 THz. It is clearly observed that AFSM exhibits a single-band and dual-band switching characteristic. At TM mode, there is one resonance for x value changing from 0 μm to 40 μm tuned from 0.33 THz to 0.45 THz. The tuning trend is nonlinear with a tuning range of 0.12 THz. Fig. 4 shows the transmission spectra of AFSM with b parameter of 70 μm and other parameters are kept as constant as $a = 40\,\mu m$, $c = 5\,\mu m$, and $d = 10\,\mu m$ at TE mode (Fig. 4(a)) and TM mode (Fig. 4(b)), respectively. In the initial state, the gap between AFSM is zero, the resonances of AFSM are 0.26 THz and 0.33 THz at TE mode and TM mode, respectively. When x value is changed from 4 μm to 40 μm, there are two resonances at TE mode. The first resonance is almost kept as constant as

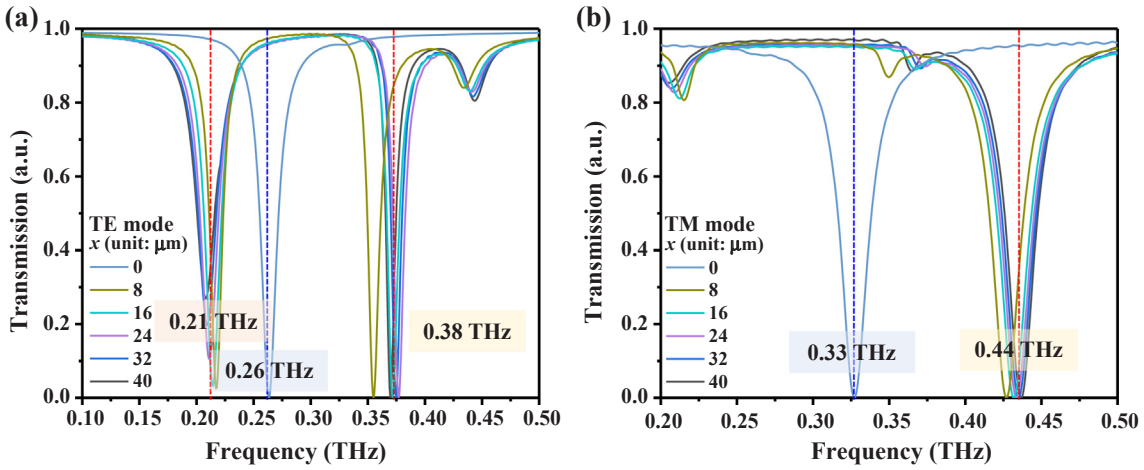

Fig. 2. Transmission spectra of AFSM with b = 60 μm at different x value from 0 μm to 40 μm at (a) TE mode and (b) TM mode.

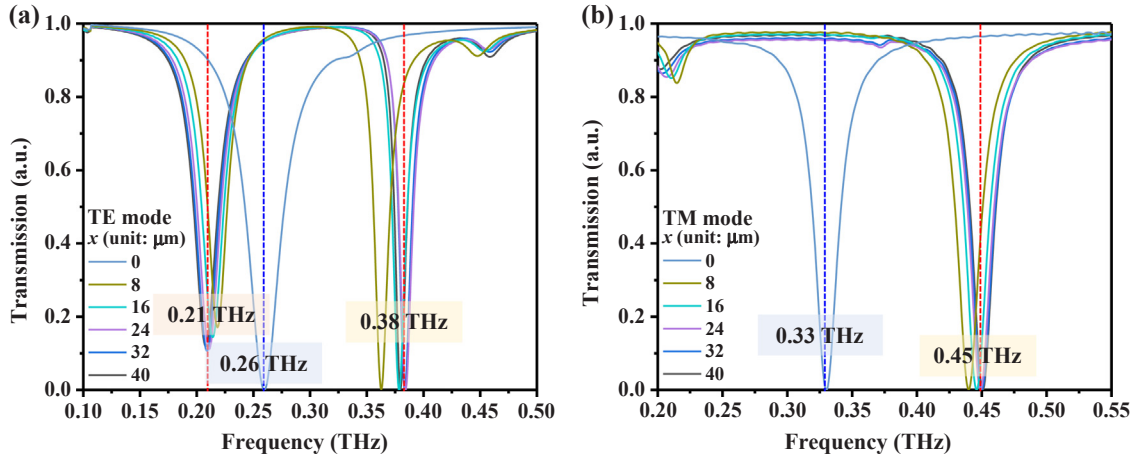

Fig. 3. Transmission spectra of AFSM with b = 65 μm at different x value from 0 μm to 40 μm at (a) TE mode and (b) TM mode.

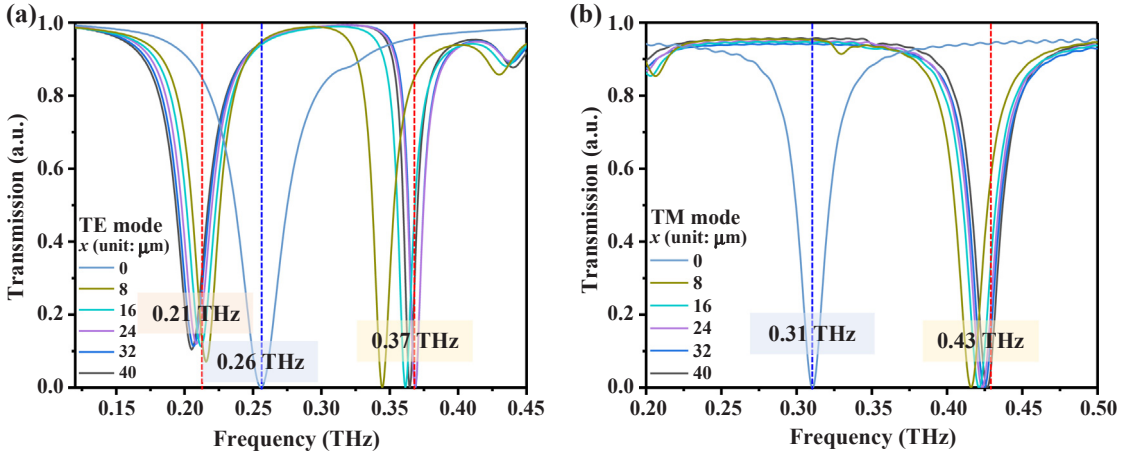

Fig. 4. Transmission spectra of AFSM with b = 70 μm at different x value from 0 μm to 40 μm at (a) TE mode and (b) TM mode.

0.21 THz and the second resonance is shifted from 0.32 THz to 0.37 THz. The tuning range is 0.05 THz. When the x value is 0 μm, there is only one resonance at 0.26 THz. It is clearly observed that AFSM exhibits a single-band and dual-band switching characteristic. At TM mode, there is one resonance for x value changing from 0 μm to 40 μm tuned from 0.31 THz to 0.43 THz. The tuning trend is nonlinear with a tuning range of 0.12 THz.

The relationships of resonances and x value for b = 60 μm, 65 μm, and 70 μm at TE and TM modes are plotted in Fig. 5(a) and (b), respectively. The resonance is blue-shift and then saturated gradually due to the F-shaped microstructure is moved to be farer than another F-shaped microstructure. To understand the physic mechanism, the corresponding electric (E) field and magnetic (H) field distributions are monitored within the F-shaped metamaterials, which are indicated in Fig. 6 for TE mode (Fig. 6(a)) and TM mode (Fig. 6(b)), respectively, where b parameter is 60 μm. In the initial state (x = 0 μm), the E-field

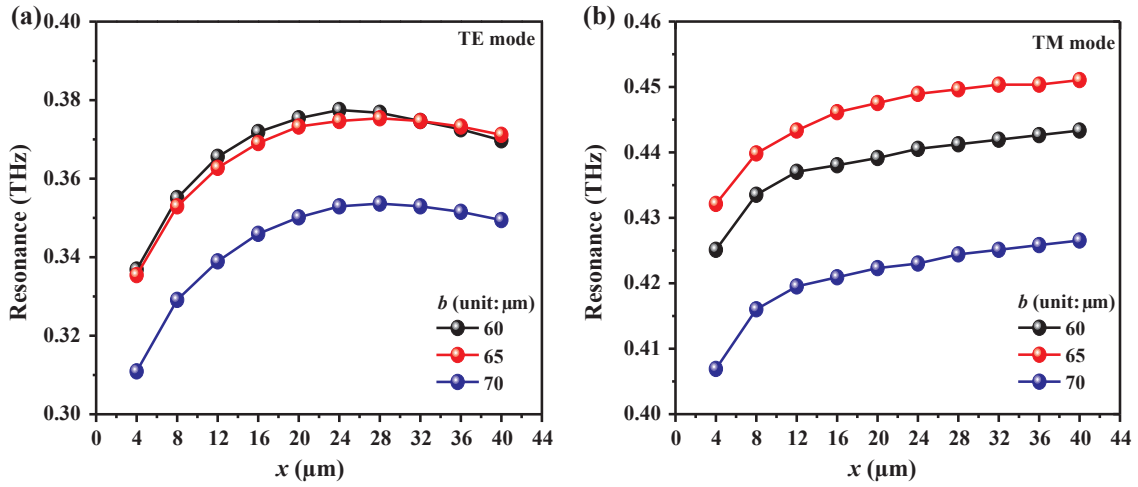

Fig. 5. The relationships of resonance and x value for b = 60 μm, 65 μm, and 70 μm at (a) TE mode and (b) TM mode, respectively.

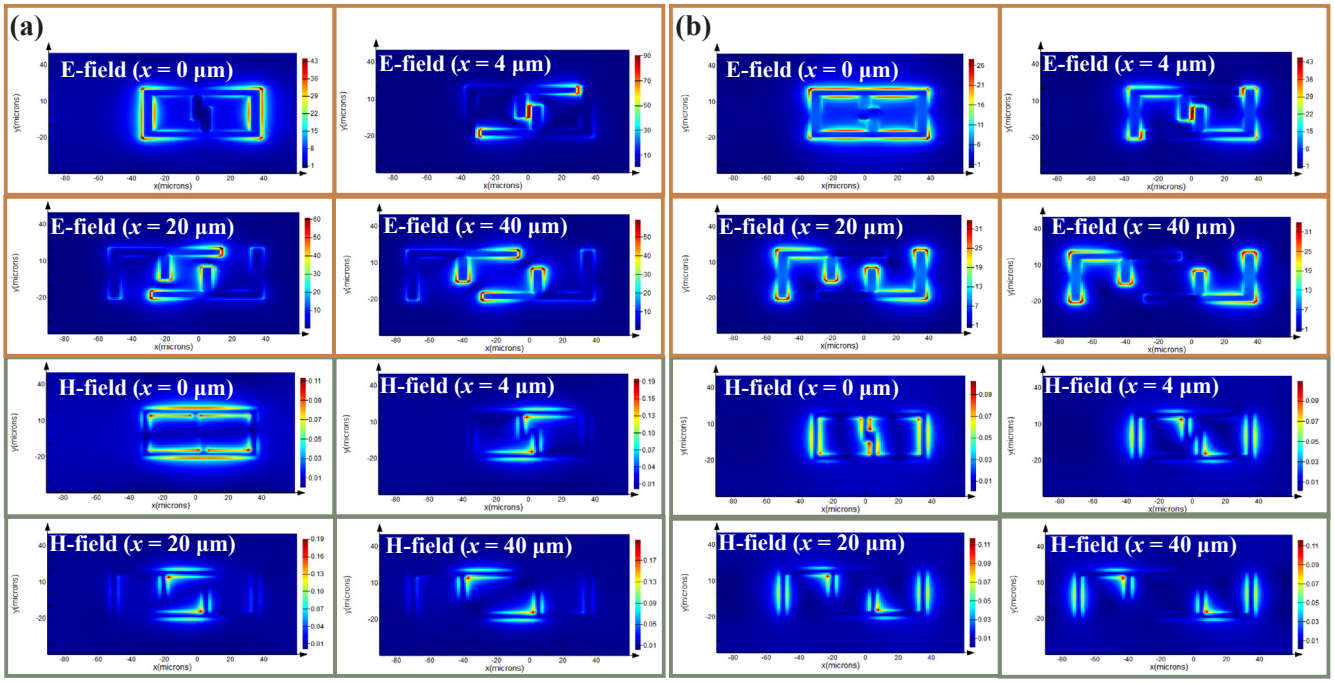

Fig. 6. E-field and H-field distributions of AFSM with different x value from 0 μm to 40 μm at (a) TE mode and (b) TM mode.

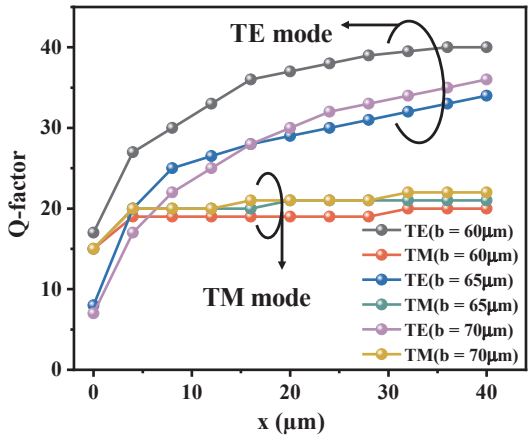

Fig. 7. The summaries of Q-factors for AFSM with different b value.

energy is distributed in the left and right two conductor bars of F-shaped microstructure, while the H-field energy is distributed around the top and bottom two conductor bars of F-shaped microstructure at TE mode. At TM mode, the E-field energy is distributed around the whole device contour, while the H-field energy is distributed in the left, middle and right conductor bars of F-shaped microstructure. When x value is changed from 4 μm to 40 μm, the E-field energy is distributed in the middle of device and the bottom of F-shaped microstructure at TE mode, while the H-filed energy is in the middle of F-shaped microstructure. At TM mode, the E-field energy is distributed in the middle of device and around the top of F-shaped microstructure, while the H-field energy is distributed around in the middle of device.

The relationships of Q-factors and x values of tunable AFSM are plotted in Fig. 7. It is clearly observed the relationships of Q-factors and x values of three AFSM devices are linear trends. These Q-factors are almost identical and kept as constant as 20 at TM mode. At TE mode, the trends of Q-factors to x values of three AFSM devices are increasing gradually as shown in Fig. 7. The corresponding slopes are 0.27, 0.30,

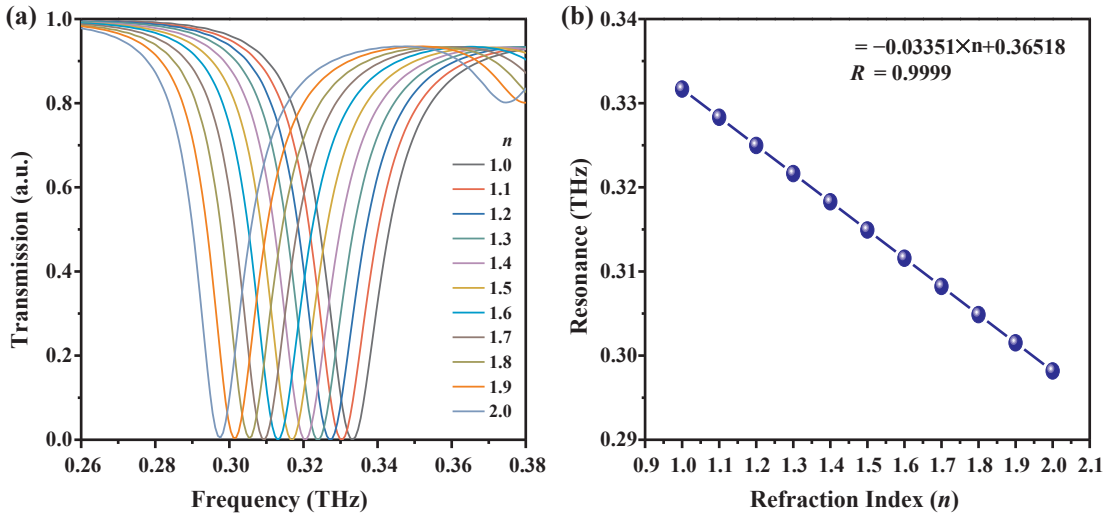

Fig. 8. (a) Transmission spectra of AFSM exposed on ambient environment with different refraction index (n) from 1.0 to 2.0. (b) The relationship of resonance and n vlaue.

and 0.42 for $b = 60\,\mu m$, $b = 65\,\mu m$, and $b = 70\,\mu m$, respectively. The average Q-factors are 37, 30, and 32 for the cases of $b = 60\,\mu m$, $b = 65\,\mu m$, and $b = 70\,\mu m$ at TE mode, respectively. The highest Q-factor is 40 for the case of $b = 60\,\mu m$ and $x = 40\,\mu m$. Such electromagnetic characteristic of ultra-high Q-factor is very suitable for the use in sensing application. To further prove the applicability of proposed tunable AFSM device, which is designed to be exposed on different ambient environmental mediums and then demonstrated the high-efficiency sensor application. Fig. 8(a) shows the transmission spectra of tunable AFSM device by changing ambient reflection index (n) from 1.0 to 2.0. The geometrical parameters are kept at $x = 4\,\mu m$, a = 40 μm, $b = 60\,\mu m$, $c = 5\,\mu m$, and $d = 10\,\mu m$, respectively. The relationship of resonance and reflection index is summarized in Fig. 8(b). The trend is linear with a correlation coefficient of 0.9999. This value is better than those reported in literatures [12–39]. Such design of tunable AFSM device can be used as a high-efficiency environmental sensor.

4. Conclusions

In conclusion, an actively tunable THz resonator by using AFSM microstructures is presented. The proposed AFSM device exhibits the tunabilities of single-band and dual-band resonances with an ultra-narrow bandwidth. The resonance could be tuned by changing the gap between F-shaped microstructures. The tuning ranges of resonances could be spanned from 0.20 to 0.40 THz to be a THz switch function. The highest Q-factor is 40 for the case of $b = 60$ at TE mode. At TM mode, Q-factors of three AFSM devices are stable and kept as constant as 20. The proposed AFSM device can be not only realized an ultra-narrowband resonator but also a THz switch and polarization switch. To enhance the flexibility of AFSM device, it is exposed on different surrounding environment with different refraction index for high-efficiency environmental sensor with a correlation coefficient of 0.9999. This work provides the detail investigation of tunable THz resonator by using AFSM microstructures. With the investigation of geometrical relationships of AFSM being fully understood, the design of AFSM provides a new direction for future THz device applications.

Acknowledgment

The authors acknowledge the financial support from research grants of 100 Talents Program of Sun Yat-Sen University (grant number 76120-18841202) and the State Key Laboratory of Optoelectronic Materials and Technologies of Sun Yat-Sen University for the use of experimental equipment.

Appendix A. Supplementary material

Supplementary data to this article can be found online at https://doi.org/10.1016/j.optlastec.2019.105826.

References

[1] Y.S. Lin, F. Ma, C. Lee, Three-dimensional movable metamaterial using electric split-ring resonators, Opt. Lett. 38 (16) (2013) 3126–3128.
[2] J.L. Huang, J.S. Liu, K.J. Wang, Z.G. Yang, X.M. Liu, Classification and identification of molecules through factor analysis method based on terahertz spectroscopy, Spectroc. Acta Pt. A-Molec. Biomolec. Spectr. 198 (2018) 198–203.
[3] R. Peretti, F. Braud, E. Peytavit, E. Dubois, J.F. Lampin, Broadband terahertz light-matter interaction enhancement for precise spectroscopy of thin films and micro-samples, Photonics 5 (2) (2018) 11.
[4] K. Ahi, S. Shahbazmohamadi, N. Asadizanjani, Quality control and authentication of packaged integrated circuits using enhanced-spatial-resolution terahertz time-domain spectroscopy and imaging, Opt. Lasers Eng. 104 (2018) 274–284.
[5] D.S. Jessop, S.J. Kindness, L. Xiao, P. Braeuninger-Weimer, H. Lin, Y. Ren, C.X. Ren, S. Hofmann, J.A. Zeitler, H.E. Beere, D.A. Ritchie, R. Degl'Innocenti, Graphene based plasmonic terahertz amplitude modulator operating above 100 MHz, Appl. Phys. Lett. 108 (17) (2016) 171101.
[6] J.J. Wang, R. Ashrafi, R. Adams, I. Glesk, I. Gasulla, J. Capmany, L.R. Chen, Subwavelength grating enabled on-chip ultra-compact optical true time delay line, Sci. Rep. 6 (2016) 30235.
[7] T. Nagatsuma, S. Hisatake, M. Fujita, H.H.N. Pham, K. Tsuruda, S. Kuwano, J. Terada, Millimeter-wave and terahertz-wave applications enabled by photonics, IEEE J. Quantum Electron. 52 (1) (2016) 0600912.
[8] C.M. Soukoulis, M. Wegener, Past achievements and future challenges in the development of three-dimensional photonic metamaterials, Nat. Photonics 5 (9) (2011) 523–530.
[9] D. Yao, K. Yan, X. Liu, S. Liao, Y. Yu, Y.S. Lin, Tunable terahertz metamaterial by using asymmetrical double split-ring resonators (ADSRRs), OSA Continuum 1 (2) (2018) 349–357.
[10] C.P. Ho, P. Pitchappa, Y.S. Lin, C.Y. Huang, P. Kropelnicki, C. Lee, Electrothermally actuated microelectromechanical systems based omega-ring terahertz metamaterial with polarization dependent characteristics, Appl. Phys. Lett. 104 (16) (2014) 161104.
[11] A. Isozaki, T. Kan, H. Takahashi, K. Matsumoto, I. Shimoyama, Out-of-plane actuation with a sub-micron initial gap for reconfigurable terahertz micro-electro-mechanical systems metamaterials, Opt. Express 23 (20) (2015) 26243–26251.
[12] Y.S. Lin, C.-Y. Huang, C. Lee, Reconfiguration of resonance characteristics for terahertz U-shape metamaterial using MEMS mechanism, IEEE J. Sel. Top. Quantum Electron. 21 (4) (2015) 2700207.
[13] R. Xu, X. Liu, Y.S. Lin, Tunable ultra-narrowband terahertz perfect absorber by using metal-insulator-metal microstructures, Results Phys. 13 (2019) 102176.
[14] P. Pitchappa, M. Manjappa, C.P. Ho, R. Singh, N. Singh, C. Lee, Active control of electromagnetically induced transparency analog in terahertz MEMS metamaterial, Adv. Opt. Mater 4 (4) (2016) 541–547.
[15] W.M. Zhu, A.Q. Liu, W. Zhang, J.F. Tao, T. Bourouina, J.H. Teng, X.H. Zhang, Q.Y. Wu, H. Tanoto, H.C. Guo, G.Q. Lo, D.L. Kwong, Polarization dependent state to polarization independent state change in THz metamaterials, Appl. Phys. Lett. 99

(22) (2011) 221102.
[16] J.J. Talghader, A.S. Gawarikar, R.P. Shea, Spectral selectivity in infrared thermal detection, Light-Sci. Appl. 1 (8) (2012) e24.
[17] C.F. Guo, T. Sun, F. Cao, Q. Liu, Z. Ren, Metallic nanostructures for light trapping in energy-harvesting devices, Light-Sci. Appl. 3 (2014) e161.
[18] Y. Yu, Y.S. Lin, Multi-functional terahertz metamaterial using symmetrical and asymmetrical electric split-ring resonator, Results Phys. 13 (2019) 102321.
[19] S. Yang, C. Tang, Z. Liu, B. Wang, C. Wang, J. Li, L. Wang, C. Gu, Simultaneous excitation of extremely high-Q-factor trapped and octupolar modes in terahertz metamaterials, Opt. Express 25 (14) (2017) 15938–15946.
[20] S. Cheng, Z. Xu, D. Yao, X. Zhang, Z. Zhang, Y.S. Lin, Electromagnetically induced transparency in terahertz complementary spiral-shape metamaterial, OSA Continuum 2 (7) (2019) 2137–2144.
[21] J.F. Zhou, T. Koschny, C.M. Soukoulis, Magnetic and electric excitations in split ring resonators, Opt. Express 15 (26) (2007) 17881–17890.
[22] M.T. Islam, M.M. Islam, M. Samsuzzaman, M.R.I. Faruque, N. Misran, A negative index metamaterial-inspired UWB antenna with an integration of complementary SRR and CLS unit cells for microwave imaging sensor applications, Sensors 15 (5) (2015) 11601–11627.
[23] L.Y.M. Tobing, Y. Luo, K.S. Low, D.W. Zhang, D.H. Zhang, Observation of the kinetic inductance limitation for the fundamental magnetic resonance in ultrasmall gold V-shape split ring resonators, Adv. Opt. Mater. 4 (7) (2016) 1047–1052.
[24] Z. Xu, Y.S. Lin, A stretchable terahertz parabolic-shaped metamaterial, Adv. Opt. Mater. 7 (12) (2019) 1900379.
[25] M.C. Wu, A. Solgaard, J.E. Ford, Optical MEMS for lightwave communication, J. Lightwave Technol. 24 (12) (2006) 4433–4454.
[26] C.Y. Chen, M.H. Li, C.H. Chin, S.S. Li, Implementation of a CMOS-MEMS filter through a mixed electrical and mechanical coupling scheme, J. Microelectromech. Syst. 25 (2) (2016) 262–274.
[27] S. Marauska, R. Jahns, H. Greve, E. Quandt, R. Knoechel, B. Wagner, MEMS magnetic field sensor based on magnetoelectric composites, J. Micromech. Microeng. 22 (6) (2012) 065024.
[28] P. Liu, Z. Liang, Z. Lin, Z. Xu, R. Xu, D. Yao, Y.S. Lin, Actively tunable terahertz chain-link metamaterial with bidirectional polarization-dependent characteristic, Sci. Rep. 9 (2019) 9917.
[29] S.C. Ambhire, S. Palkhivala, A. Agrawal, A. Gupta, G. Rana, R. Mehta, D. Ghindani, A. Bhattacharya, V.G. Achanta, S.S. Prabhu, “Pattern and Peel” method for fabricating mechanically tunable terahertz metasurface on an elastomeric substrate, Opt. Mater. Express 8 (11) (2018) 3382–3391.
[30] L.J. Liang, B.B. Jin, J.B. Wu, G.C. Zhou, Y.G. Zhang, X.C. Tu, T. Jia, X.Q. Jia, C.H. Cao, L. Kang, W.W. Xu, J. Chen, Terahertz narrow ban.dstop, broad bandpass filter using double-layer S-shaped metamaterials, Sci. China-Inf. Sci. 56 (12) (2013) 120412.
[31] C. Liu, Y. Huang, Z. Yao, L. Yu, Y. Jin, X. Xu, Giant angular dependence of electromagnetic induced transparency in THz metamaterials, EPL 121 (4) (2018) 44004.
[32] C. Rockstuhl, T. Paul, F. Lederer, T. Pertsch, T. Zentgraf, T. Meyrath, H. Giessen, Transition from thin-film to bulk properties of metamaterials, Phys. Rev. B 77 (2008) 035126-1–035126-9.
[33] Z.G. Dong, S.N. Zhu, H. Liu, J. Zhu, W. Cao, Numerical simulations of negative-index refraction in wedge-shaped metamaterials, Phys. Rev. E 72 (2005) 016607-1–016607-4.
[34] L. Markley, G.V. Eleftheriades, A negative-refractive-index metamaterial for incident plane waves of arbitrary polarization, IEEE Antennas Wireless Propag. Lett. 6 (2007) 28–32.
[35] T.D. Karamanos, A.I. Dimitriadis, N.V. Kantartzis, Compact double-negative metamaterials based on electric and magnetic resonators, IEEE Antennas Wireless Propag. Lett. 11 (2012) 480–483.
[36] R. Liu, A. Degiron, J.J. Mock, D.R. Smith, Negative indexmaterial composed of electric and magnetic resonators, Appl. Phys. Lett. 90 (2007) 263504-1–263504-3.
[37] A. Alù, N. Engheta, A. Erentok, R.W. Ziolkowski, Single-negative, double-negative, and low-index metamaterials and electromagnetic applications, IEEE Antennas Propag. Mag. 49 (1) (2007) 23–36.
[38] T.D. Karamanos, S.D. Assimonis, A.I. Dimitriadis, N.V. Kantartzis, Effective parameter ex-traction of 3D metamaterial arrays via first-principles homogenization theory, Photonics Nanostruct. – Fundam. Appl. 12 (4) (2014) 291–297.
[39] C.M. Soukoulis, M. Kafesaki, E.N. Economou, Negative-index materials: new frontiers in optics, Adv. Mater. 18 (15) (2006) 1941–1952.
[40] Y.Z. Cheng, Y. Nie, R.Z. Gong, A polarization-insensitive and omnidirectional broadband terahertz metamaterial absorber based on coplanar multi-squares films, Opt. Laser Technol. 48 (2013) 428–435.
[41] Y.S. Lin, K.H. Yan, D.Y. Yao, Y.B. Yu, Investigation of electromagnetic response of terahertz metamaterial by using split-disk resonator, Opt. Laser Technol. 111 (2019) 509–514.